Special Issue of the International Conference on Research and Applications of Plasmas (PLASMA-2019)

Characteristics of VHF Discharge N_2 Plasma in Uragan-2M Stellarator

Yu.V. Kovtun[a,*], V.E. Moiseenko[a], A.V. Lozin[a], A.N. Shapoval[a], L.I. Grigor'eva[a], V.B. Korovin[a], E.D. Kramskoy[a], M.M. Kozulya[a],G.P. Glazunov[a], M.N. Bondarenko[a], D.I. Baron[a], A.A. Bizyukov[b] and Uragan-2M Team

[a] *Institute of Plasma Physics of the NSC KIPT, 1 Akademichna Str., 61108 Kharkiv, Ukraine*
[b] *Karazin Kharkiv National University, 4 Svobody Sq., 61022 Kharkiv, Ukraine*

Doi: 10.12693/APhysPolA.138.632 *e-mail: Ykovtun@kipt.kharkov.ua

The very high frequency (VHF) discharge for wall conditioning in nitrogen atmosphere is studied. The wall conditioning is applied together with baking. It is driven by the radio frequency (RF) power at the frequency of 130 MHz, higher than that usually used in ion cyclotron resonance heating. The volumetric VHF discharge is successfully ignited and stationary sustained, and plasma occupies most of the vacuum chamber volume. The Langmuir probe measurements give the plasma density and electron temperature. In the optical emission spectrum of the plasma, lines N_2, N_2^+ and the cyano (CN) radical are observed. Possible mechanisms for the formation of the CN radical in the discharge are discussed.

topics: wall conditioning, radio-frequency discharge, stellarator, slow wave

1. Introduction

Decreasing the inflow of light and heavy impurities into the plasma column is of importance in high-temperature plasma experiments which are aimed at investigating conditions for controlled fusion. After toroidal current disruptions in tokamaks and radiation collapses in stellarators, plasma parameters decrease and high energy losses are caused by extraneous matter getting into plasma from the inner walls of the vacuum chamber. This is the reason why an inner vacuum surface conditioning is the integral part of the experiments in fusion devices. The wall conditioning in magnetic fusion devices is also used after deconditioning events, such as leaks and opening the vacuum chamber to air, and during the machine operational phase to remove impurities that migrate to the vacuum chamber from hidden places. A variety of inner vacuum chamber surfaces conditioning methods are used [1–3]: surface conditioning by pulsed and continuous plasma discharges such as the Taylor discharge cleaning [1–3], radio-frequency-assisted glow discharge [2, 3], glow discharge conditioning [1–5], RF discharges [6–9] at different frequency bands (electron cyclotron [4, 5, 10] and ion cyclotron [10, 11] wall conditioning) and conditioning with noble (He [4, 5], Ne, Ar [12]), chemically active gases (H_2, O_2 [2, 3], N_2) and their mixtures [11].

The technology of plasma surface conditioning with continuous very high frequency (VHF) discharge was proposed and tested in stellarator (torsatron) Uragan-2M [13]. The discharge was previously sustained with the small antenna of different modifications [13, 14] while this study employs a newly developed T-shaped antenna [15] (see Sect. 3). This technology features the possibility of its usage in the wide range of magnetic fields which is important for superconductive devices since it is possible to do wall conditioning in the same magnetic field in which the device operates. The previous VHF discharge experiments were carried out in pure hydrogen and hydrogen–nitrogen mixture [13–15]. The results published in [13–16] demonstrated that continuous VHF discharge plasma conditioning allows for decreasing residual gases pressure and improving vacuum conditions, decreasing outgassing inside a vacuum chamber. The estimation of the number of molecular layers method thermal desorption probe demonstrated their decrease [16].

2. VHF discharge

The VHF discharge relies upon the slow wave in magnetized plasma, the dispersion equation for which is:

$$k_\perp^2 = -\frac{\varepsilon_\parallel}{\varepsilon_\perp}\left(k_\parallel^2 - k_0^2\varepsilon_\perp\right), \tag{1}$$

where $\varepsilon_\perp = (\boldsymbol{E}\times\boldsymbol{B})\cdot\hat{\boldsymbol{\varepsilon}}\cdot(\boldsymbol{E}\times\boldsymbol{B})/|\boldsymbol{E}\times\boldsymbol{B}|^2$ and $\varepsilon_\parallel = \boldsymbol{B}\cdot\hat{\boldsymbol{\varepsilon}}\cdot\boldsymbol{B}/B^2$ are, respectively, the perpendicular and parallel dielectric tensor components, $\boldsymbol{B}$ is the steady magnetic field and $k_0 = \omega/c$. If the wave frequency is higher than the ion cyclotron frequency,

the short slow waves propagate in a cold plasma when $\varepsilon_\perp > 0$. The parallel dielectric tensor component value $\varepsilon_\parallel < 0$ is negative and mainly determined by the plasma electrons. Then, the propagation condition is satisfied if the parallel wavelength is short $k_\parallel^2 > k_0^2\varepsilon_\perp$. Since the frequency is higher than the ion cyclotron frequency ω_{ci}, the plasma contribution to $\varepsilon_\perp$ is negative and increases with plasma density.

If $\omega^2 \gg \omega_{ci}^2$, $\varepsilon_\perp$ turns zero at the layer, where $\omega \approx \omega_{pi}$ (here ω_{pi} is the ion plasma frequency) and this condition determines the highest plasma density achievable. For the frequency of 130 MHz, the maximum density is quite high — it is 1×10^{19} m^{-3} for nitrogen. This value could be reached if the power launched is much higher than the power available in the present experiment. The perpendicular component of the dielectric tensor ranges in $0 < \varepsilon_\perp < 1$ and in the plasma with noticeable density ($\omega^2 \ll \omega_{pe}^2$) the parallel component has a much bigger value $|\varepsilon_\parallel| \gg 1$. In such conditions, the perpendicular wavelength is much shorter than the parallel $k_\perp^2 \gg k_\parallel^2$. The slow wave can exist with very high $k_\parallel$ and $k_\perp$. In this case, it becomes almost electrostatic and it is difficult to couple it with antenna currents.

The wave dispersion (1) depends very weakly on the steady magnetic field. The dependence is through $\varepsilon_\perp$ variation but it is small if $\omega^2 \gg \omega_{ci}^2$ or $\varepsilon_\perp \approx 1$. The influence of gas composition on the dispersion is also through $\varepsilon_\perp$. It is strong if $\varepsilon_\perp$ differs from unity and weak if it is close to unity.

For the considered VHF discharge, the collisionless mechanisms of wave dumping are negligibly small and the wave is weakly damped owing to binary collisions of electrons mainly with the neutral gas molecules. The major contribution to the collisional damping of the wave is made by the imaginary part of $\varepsilon_\parallel \mathrm{Im}(\varepsilon_\parallel) \approx -(\nu_{en}/\omega)\mathrm{Re}(\varepsilon_\parallel - 1)$, where ν_{en} is the electron-neutral collision frequency.

In the plasma column, the slow wave forms eigenmodes (cavity modes). There are many of them since the length of the slow wave is much shorter than the plasma column size. When the heating frequency is close to the eigenmodes frequency, the global resonance occurs which results in the increase of the electromagnetic field amplitude. Because of small damping, each resonance broadening is small but since there are many resonances, neighbouring resonances can overlap. The overlapping of the resonances provides good and stable antenna coupling to plasma [13].

3. T-shaped antenna

The T-shaped antenna [15] is specially designed for the VHF discharge. It comes to replace small-frame antennas used before. The frame antennas were grounded and for this reason received a lot of heat. The T-shaped antenna is a monopole and has a floating potential in plasma. The sketch of

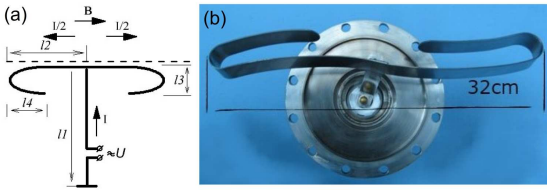

Fig. 1. T-shaped antenna: (a) sketch and (b) photo.

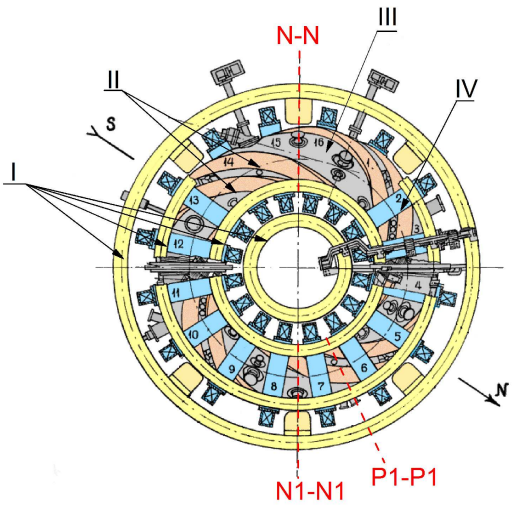

Fig. 2. Scheme of Uragan-2M. I — poloidal field coils, II — helical field coils, III — power frame, IV — toroidal field coils numbered 1–16. N–N, P1–P1, N1–N1 — diagnostic cross-sections.

this antenna is shown in Fig. 1. It is fed through the coaxial feed-through to the central conductor of length l_1. Then the conductor splits in two straps oriented along the magnetic field, each of length l_2. As it is assumed, these two straps excite the slow waves with the characteristic longitudinal wave number $k_\parallel = \pi/l_2$. The bent part is attached to each strap end (lengths are l_3 and l_4). The sizes of the T-shaped antenna are chosen in such a way that $l_1 + l_2 + l_3 + l_4 = \pi/(2k_0)$. In this case, a simple antenna matching circuit can be used.

The T-shaped antenna is made of a stainless steel strap 20 mm wide and 2 mm thick. Top of the antenna is shaped according to plasma column surface along the magnetic field lines. The distance between it and the last closed magnetic surface (LFS) is 15 mm. The antenna is placed at LFS and occupies the port at the N–N cross-section (see Fig. 2). This location is quite a distance away from the limiter which is located between coils No. 10 and 11.

4. Experiment and diagnostic methods

4.1. Experimental setup

The VHF discharge nitrogen plasma studies were performed at Uragan-2M device (U-2M) [17–21]. The medium-sized torsatron type stellarator U-2M was assembled in the early 1990s [17, 18]. U-2M

was finally built and put into operation at the end of 2006 [19, 20]. The U-2M stellarator scheme is shown in Fig. 2. The major radius of the device is $R = 1.7$ m, the average plasma radius $r_{pl} < 24$ cm and the toroidal magnetic field $B_0 < 0.6$ T. The U-2M magnetic system consists of $l = 2$ helical coils with four periods ($m = 4$) in toroidal direction and the minor radius of the helical coils is $r_h = 0.44$ m. The toroidal magnetic field is provided by the set of 16 circular toroidal coils evenly distributed along the tore axis; the set of poloidal coils is for compensation of the vertical magnetic field induced by the helical coils and for the control of the plasma column position. The toroidal vacuum chamber minor radius is $r_c = 0.34$ m, the volume is $V_c = 3.88$ m^3 (without vacuum ports) and the inner surface area is $S = 22.8$ m^2. There are 48 ports used for diagnostics, gas puffing and vacuum pumping. The vacuum chamber is pumped by three turbo-molecular pumps TMP-500, each with the pumping rate of 0.5 m^3/s and equipped with liquid N_2 cryotraps.

4.2. Diagnostic methods

The VHF discharge local plasma parameters (the electron temperature and plasma density) were measured with single cylindrical Langmuir probes placed in different points inside the toroidal chamber (see Fig. 3). Probe 1 was located near the antenna in the cross-section N–N and probes 2–4 were located in the cross-section N1–N1.

The ions charge state and plasma elemental composition were determined through the optical emission spectroscopy. The plasma line spectrum in 214–673 nm spectral range was detected with SL-40-2-3648 USB spectrometer SOLAR TII (spectral resolution < 0.6 nm). The spectrometer was located in the cross-section P1–P1. Spectral lines were identified according to the data from [22, 23]. The volume averaged electron temperature was determined by spectral line intensity ratio (line-ratio method) [24]. It was assumed that the plasma is

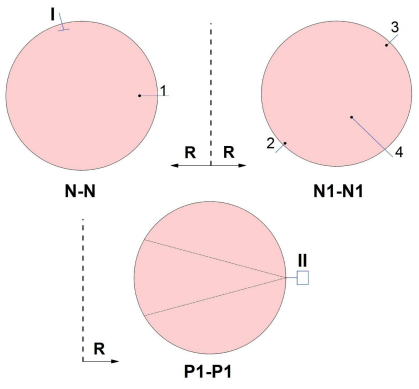

Fig. 3. Diagnostic cross-sections N–N, N1–N1, P1–P1. 1–4 — single Langmuir probes (point–probe position), I — T-shaped antenna, II — optical spectrometer.

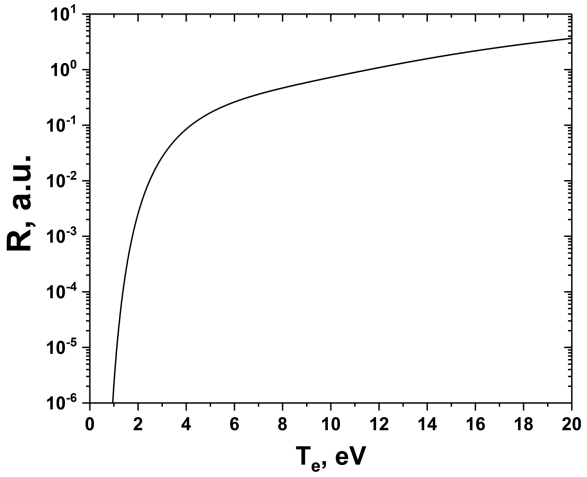

Fig. 4. Ratios of the excitation rate coefficients (excitation cross-sections [25]) from the ground state as functions of electron temperature $N_2^+(B^2\Sigma_u^+, v = 0)$ / $N_2(C^3\Pi_u, v = 0)$.

optically transparent and the electron energy distribution function is Maxwellian; the main input into excited level population is made by electron impact from the N_2 ground state. The nitrogen discharge electron temperature was determined by 391.4 nm $N_2^+(B^2\Sigma_u^+, v = 0)$ and 337.03 nm $N_2(C^3\Pi_u, v = 0)$ spectral line intensity ratio. The calculated N_2 ground state excitation rate constant dependence on electron temperature is shown in Fig. 4 and $N_2^+(B^2\Sigma_u^+, v = 0)$ and $N_2(C^3\Pi_u, v = 0)$ levels of excitation cross-sections were taken from paper [25].

The partial pressure of residual gases in the U-2M vacuum chamber was measured with "IPDO-2" (partial pressure meter omegatron OPPM-2) omegatron type mass-spectrometer with omegatron tube "RMO–4S" (resonant radio frequency mass spectrometer) [26, 27]. Its characteristics allow for measurements of partial pressures of residual gases without calibration with an accuracy of about 25%. If necessary, it is possible to achieve an accuracy of 10% using the calibration procedure for one pure gas. For the quantitative analysis of gas mixtures taking into account the processes of formation of fragmentation and multiply charged ions, the method described in [28] was used. In this case, a system of linear equations is solved that relates the values of the output signals of the mass spectrometer to the partial pressures of the individual components of the analyzed gas mixtures.

4.3. Experimental arrangements

The helical and toroidal coils have created a magnetic field $B_0 \approx 0.01$ T and a low power direct-current source is used as a power supply. In this case, the plasma will fill the chamber volume more evenly and the particle flow to the chamber wall should be more uniform. This is a favorable factor for a vacuum chamber conditioning.

The vacuum chamber was heated to degas surfaces and activate chemical processes on the surface with chemically active gases. Nitrogen was the working gas that was continuously puffed into the vacuum volume, keeping the pressure $P_{\text{o.p.}} = 4 \times 10^{-2}$ Pa, then stationary discharge has started after 25 h of baking, as the chamber wall temperature reached 70–80 °C.

The frame antenna RF pulse caused the breakdown of the gas [8] and created initial plasma with the density of up to 1×10^{18} m^{-3} with impulse RF-discharge (t = 20 ms, f = 5.4 MHz) [21]. The VHF generator has been turned on just before the initial plasma creation and sustained a stationary discharge for a long time (120 min). The VHF power up to $P_{\text{RF}} = 3$ kW at the power of frequency f = 130 MHz was transmitted from the generator to the T-shaped antenna over the feeder line. The VHF discharge can be ignited independently without pre-ionization by a temporal gas pressure increase to $P_{\text{o.p.}} < 10^{-1}$ Pa.

5. Results and discussion

The composition and partial pressure of residual gases (Fig. 5) were determined with the mass-spectroscopy method before a nitrogen puff into the chamber. The estimate shows that the nitrogen to residual gas pressure ratio is ≈ 400 after nitrogen puff to the pressure of 10^{-2} Pa.

The characteristic plasma density, floating potential and electron temperature measured with the Langmuir probes are given in Table I. The averaged electron temperature determined through spectral lines ratio as 11 eV matches probe measurements. As it is reported by the diagnostics and also visual investigations, the VHF discharge is a volumetric discharge as plasma occupies most of the vacuum chamber volume. The plasma has a low temperature and degree of ionization ≈ 5.2×10^{-4}. It is possible to estimate N_2^+ ions flow to the chamber wall basing on the probe 2 data as 2.3×10^{19} m^{-2} s^{-1} ($\Gamma_i = N_i v_s$, where v_s is the ion sound velocity and N_i is the ion density $N_i \approx N_e$).

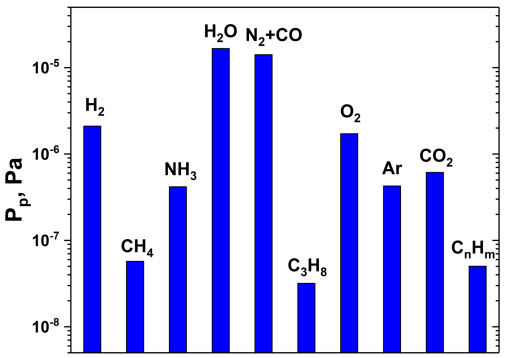

Fig. 5. Partial pressures of residual gas components (vacuum chamber temperature 80 °C, pressure in vacuum chamber $P_{\text{i.p.}} = 9.1 \times 10^{-5}$ Pa).

Plasma parameters. TABLE I

Single Langmuir probe No.	Minor radius position [cm]	V_{fl} [V]	T_e [eV]	N_e [m^{-3}]
1	26	−3.4	8.5	4.3×10^{15}
2	33	−6.8	10	3.9×10^{15}
3	32	−3.2	8	4.2×10^{15}
4	13	−5.4	10	1.7×10^{15}

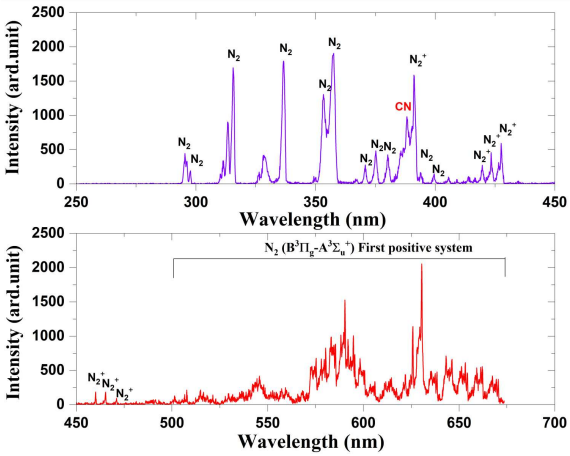

Fig. 6. Optical emission spectra of N_2 plasma.

N_2 and N_2^+ lines (working gas) are observed in the optical emission spectrum of the plasma as well as the CN radical (see Fig. 6). The formation of the CN radical is possible in various plasma chemical reactions with carbon-containing plasma contaminants. CN volatile species formation is also possible in the interactions of nitrogen with impurities (carbon-containing) accumulated on the surface.

It was shown in [29] that CN, C_2N_2, HCN and HOCN are formed during the chemical sputtering of carbon films. CN, C_2N_2 and HCN and other chemical etching products were observed during the etching of a-C:H films in N_2 plasma in [30]. Also, in [31], when cleaning a-C:H films in glow discharge plasma (H_2/N_2), C_2N_2 and HCN were observed. The measured a-C:H films N_2^+ ions chemical etching coefficient in the 30 to 900 eV energy range is considerably higher than the calculated physical sputtering coefficient of carbon with N_2^+ ions [32]. The chemical sputtering coefficient is ≈ 0.3 at the ion energy 30 eV, while the same physical sputtering coefficient is reached at the ion energy of 300 eV [32].

The residual gas pressure decreased from $P_{\text{i.p.}} = 4 \times 10^{-5}$ Pa to 1.7×10^{-5} Pa and partial pressure of residual gases changed (see Fig. 7) as a result of VHF discharge nitrogen plasma chamber conditioning (12 h total) and heating the chamber (11 h of heating to T = 70–80 °C, +69 h of stationary temperature, +11 h of cooling down).

As can be seen from Fig. 7, as a result of cleaning, the partial pressures of water, N_2 + CO, NH_3 and heavy hydrocarbons decrease by 52.9%, 38.6%,

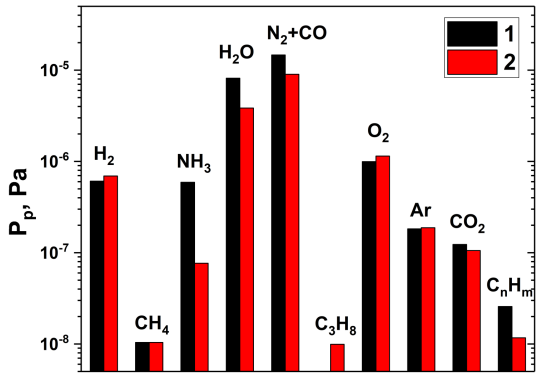

Fig. 7. Partial pressures of residual gas components. 1 — before baking and conditioning ($P_{\text{i.p.}} = 4 \times 10^{-5}$ Pa) 18.01.2019, 2 — after baking and conditioning ($P_{\text{i.p.}} = 1.7 \times 10^{-5}$ Pa) 25.01.2019.

87% and 54.6%, respectively. As experiments show, in the plasma of the H_2/N_2 mixture, ammonia is formed [33–35]. The maximum concentration of NH_3 is observed at fairly high percentages of hydrogen in nitrogen or nitrogen in hydrogen (tens of percent). In these experimental conditions, hydrogen is a very small addition to nitrogen (the concentration of hydrogen is of a smaller order of magnitude than the concentration of nitrogen). The lines of H_2 (H) and NH are not observed in the optical emission spectrum. Accordingly, the production of NH_3 in the discharge plasma is small and the concentration will depend on the balance of the processes of generation and loss (including vacuum pumping) of ammonia. The partial pressures of hydrogen, oxygen, argon and CO_2 increase by 13.8%, 15.3%, 2.9% and 14.3%, respectively. These values are within the measurement error.

6. Conclusion

The VHF discharge for wall conditioning in nitrogen atmosphere is studied. Nitrogen is chosen for its chemical activity and lower ability to penetrate into the wall material as compared with hydrogen. The wall conditioning is applied together with baking. This allows for combining a decrease of the water amount in the vacuum chamber with an increase, due to high temperature, of the probability of chemical reactions of nitrogen atoms and ions with impurities accumulated at the plasma facing components (PFC). The volumetric VHF discharge is successfully ignited and stationary sustained, and plasma occupies most of the vacuum chamber volume. The probe measurements give the values of plasma density and electron temperature. The characteristic plasma densities are $(1.7–4.2) \times 10^{15}$ m^{-3} and the electron temperature varies in the range of 8–10 eV. This temperature is in consistency with the estimates made from optical measurements. In the discharge in hydrogen [15], the value of the plasma density is three times higher and the electron temperature is also higher. This fact could probably be explained with the same argument as in [36]: higher radiation cooling in case of nitrogen. The N_2, N_2^+ lines as well as the CN radical are observed in the optical emission spectrum of the plasma. The formation of the CN radical is possible in various plasma chemical reactions with carbon-containing gas substances and also in the interactions of nitrogen with the impurities (carbon-containing) on the vacuum chamber surface.

Acknowledgments

This work has been carried out within the framework of the EUROfusion Consortium and has received funding from the Euratom research and training programme 2014–2018 and 2019–2020 under grant agreement No. 633053. The views and opinions expressed herein do not necessarily reflect those of the European Commission.

This work has also received funding from the National Academy of Sciences of Ukraine (grants P-3-22 and CV-5-20).

Authors are thankful to Dr. V.S. Voitsenya for his comments.

References

[1] H.F. Dylla, *J. Nucl. Mater.* **93**, 61 (1980).

[2] J. Winter, *J. Nucl. Mater.* **161**, 265 (1989).

[3] J. Winter, *Plasma Phys. Control. Fusion* **38**, 1503 (1996).

[4] T. Wauters, R. Brakel, S. Brezinsek et al., *Nucl. Fusion* **58**, 066013 (2018).

[5] T. Wauters, A. Goriaev, A. Alonso et al., *Nucl. Mater. Energy* **7**, 235 (2018).

[6] N.I. Nazarov, V.V. Plyusnin, T.Yu. Ranyuk, *Plasma Phys.* **13**, 1511 (1987).

[7] V.E. Moiseenko, P.Ya. Burchenko, V.V. Chechkin et al., in: *36th EPS Conf. on Plasma Physics, Sofia*, Vol. 33E, ECA, 2009, p. 5.199.

[8] A.V. Lozin, V.E. Moiseenko, L.I. Grigor'eva et al., *Plasma Phys. Rep.* **39**, 624 (2013).

[9] T. Wauters, D. Borodin, R. Brakel et al., *Plasma Phys. Control. Fusion* **62**, No. 3 (2020).

[10] E. De La Cal, E. Gauthier, *Plasma Phys. Control. Fusion* **47**, 197 (2005).

[11] G. Sergienko, A. Lyssoivan, V. Philipps et al., *J. Nucl. Mater.* **390**, 976 (2009).

[12] K. Nishimura, N. Ashikawa, S. Masuzaki et al., *J. Nucl. Mater.* **337-339**, 431 (2005).

[13] V.E. Moiseenko, A.V. Lozin, V.V. Chechkin et al., *Nucl. Fusion* **54**, 033009 (2014).

[14] A.V. Lozin, V.E. Moiseenko, M.M. Kozulya et al., *Probl. At. Sci. Technol. Ser. Plasma Phys.* **6**, 60 (2016).

[15] A.V. Lozin, M.M. Kozulia, V.B. Korovin et al., *Probl. At. Sci. Technol. Ser. Plasma Phys.* **6**, 50 (2018).

[16] G.P. Glazunov, D.I. Baron, V.E. Moiseenko, M.N. Bondarenko, A.L. Konotopskiy, A.V. Lozin, A.I. Lyssoivan, T. Wauters, I.E. Garkusha, *Fusion Eng. Des.* **137**, 196 (2018).

[17] V.E. Bykov, A.V. Georgievskij, V.V. Demchenko et al., *Fusion Technol.* **17**, 140 (1990).

[18] O.S. Pavlichenko, U-2M group, *Plasma Phys. Control. Fusion* **35**, B223 (1993).

[19] V.E. Moiseenko, Yu.S. Stadnik, O.M. Schvets, K.N. Stepanov, E.D. Volkov, V.I. Tereshin, *AIP Conf. Proc.* **933**, 115 (2007).

[20] A.A. Beletskii, V.L. Berezhnyj, P.Ya. Burchenko et al., *Probl. At. Sci. Technol. Ser. Plasma Phys.* **6**, 13 (2008).

[21] V.E. Moiseenko, A.V. Lozin, M.M. Kozulia, Yu.K. Mironov, V.S. Romanov, V.G. Konovalov, A.N. Shapoval, *Ukr. J. Phys.* **62**, 311 (2017).

[22] A. Lofthus, P.H. Krupenie, *J. Phys. Chem. Ref. Data* **6**, 113 (1977).

[23] R.W.B. Pearse, A.G. Gaydon, *The Identification of Molecular Spectra*, 4th ed., Chapman & Hall, 1976.

[24] X.M. Zhu, Y.K. Pu, *J. Phys. D Appl. Phys.* **43**, 403001 (2010).

[25] T. Tabata, T. Shirai, M. Sataka, H. Kubo, *At. Data Nucl. Data Tables* **92**, 375 (2006).

[26] A.P. Averina, *Pribory i Tekhnika Eksperimenta* **3**, 123 (1962) (in Russian).

[27] A.P. Averina, L.N. Linnik, G.I. Nikitina, *Pribory i tekhnika eksperimenta* **4**, 5 (1965) (in Russian).

[28] G.L. Saksaganski, Yu.N. Kotel'nikov, M.D. Maneev, G.V. Smirnitskaya, V.B. Yuferov, *Ultrahigh Vacuum in Radiophysical Apparatus Building*, Atomizdat, Moscow 1976 (in Russian).

[29] P. Hammer, W. Gissler, *Diam. Relat. Mater.* **5**, 1152 (1996).

[30] J. Hong, G. Turban, *Diam. Relat. Mater.* **8**, 572 (1999).

[31] J.A. Ferreira, F.L. Tabares, D. Tafalla, *J. Nucl. Mater.* **363-365**, 888 (2007).

[32] W. Jacob, C. Hopf, M. Schlüter, *Appl. Phys. Lett.* **86**, 204103 (2005).

[33] C.S. Moon, K. Takeda, S. Takashima, M. Sekine, Y. Setsuhara, M. Shiratani, M. Hori, *J. Appl. Phys.* **107**, 103310 (2010).

[34] A. Dalke, I. Burlacov, S. Hamann, A. Puth, J. Böcker, H.-J. Spies, J. Röpcke, H. Biermann, *Surf. Coat. Technol.* **357**, 1060 (2019).

[35] T. Body, S. Cousens, J. Kirby, C. Corr, *Plasma Phys. Control. Fusion* **60**, 075011 (2018).

[36] S. Möller, T. Wauters, A. Kreter, P. Petersson, A.G. Carrasco, *J. Nucl. Mater.* **463**, 1109 (2015).